Visual Abstract

Synthesis, microstructural characterization, mechanical, fractographic and wear behavior of micro B_4C particles reinforced Al2618 alloy aerospace composites

G. Veeresha, B. Manjunatha
Department of Mechanical Engineering, New Horizon College of Engineering, Bangalore-560103, VTU, Karnataka, India
veermech87@gmail.com, manjunatha.princi@gmail.com

V. Bharath
Department of Mechanical Engineering, Sri Venkateshwara College of Engineering, Bengalru-562157, VTU, Karnataka, India
bharathv88@gmail.com, http://orcid.org/0000-0001-6765-4728

Madeva Nagaral
Aircraft Research and Design Centre, Hindustan Aeronautics Limited, Bangalore 560037, Karnataka, India
madev.nagaral@gmail.com, http://orcid.org/0000-0002-8248-7603

V. Auradi
Department of Mechanical Engineering, Siddaganga Institute of Technology, Tumakuru-572103, Karnataka, India
vsauradi@gmail.com, http://orcid.org/0000-0001-6549-6340

ABSTRACT. In the current studies an investigations were made to know the effect of 63 micron sized B_4C particles addition on the mechanical and wear behavior of aerospace alloy Al2618 metal composites. Al2618 alloy with different weight percentages (2, 4, 6 and 8 wt. %) of 63 micron sized B_4C particles reinforced composites were produced by stir cast process. These synthesized composites were tested for various mechanical properties like hardness, compression strength and tensile behavior along with density measurements. Further, microstructural characterization was carried by SEM/EDS and XRD analysis to know the micron sized particles distribution and phases. Wear behavior of Al2618 alloy with 2 to 8 wt. % of B_4C composites were studied as per ASTM G99 standards with varying loads and sliding speeds. By adding 63 micron sized B_4C particles hardness, compression and tensile strength of Al2618 alloy was enriched with slight decrease in elongation. Further, wear resistance of Al2618 alloy was enriched with the accumulation of B_4C particles. As load and speed on the specimen increased, there was increase in wear of Al2618 alloy and its composites. Various tensile fracture surface morphology and worn surface behavior was observed by SEM analysis.

Citation: Veeresha, G, Manjunatha, B., Bharath, V., Nagaral, M, Auradi, V., Synthesis, Microstructural Characterization, Mechanical, Fractographic and Wear Behavior of Micro B4C Particles Reinforced Al2618 Alloy Aerospace Composites, Frattura ed Integrità Strutturale, 62 (2022) 385-407.

Received: 28.04.2022
Accepted: 19.08.2022
Online first: 01.09.2022
Published: 01.10.2022

KEYWORDS. Al2618 Alloy; B_4C; Microstructure; Mechanical and Wear Properties; Fractography; Worn Morphology.

INTRODUCTION

MMCs (metal matrix composites) are typically made up of two phases [1]. The first is a reinforcement phase, and the second is a matrix phase, which is usually a metallic alloy. This combining of two unique phases is done to produce material qualities that cannot be attained by a single phase, as well as to improve the composites' mechanical properties [2, 3]. Researchers are concentrating their efforts on reinforcing development in order to create high-strength MMCs. Other merits such as wear confrontation, stiffness, coefficient of thermal expansion, high temperature conduction, and so on can be achieved by including reinforcements in the matrix phase. In order to generate a desirable metal matrix composite, it is critical to use the right filler material [4].

Aluminium is well-known for its low density and ability to protect itself from corrosion through the process of passivation [5]. Because of its high specific strength to weight ratio, ease of machinability and formability, and lower cost than other materials, aluminium and aluminium alloys are particularly essential in the automobile and aeronautic industries. Due to the strong need for enhanced strength to weight ratio in aluminium alloys, a great deal of research is being done in this area by adding very high strength material reinforcement in aluminium alloys [6, 7]. The mechanical characteristics of these reinforcement materials will be altered in the desired way. As research in this area advanced, combining reinforcing components with base materials such as aluminium alloys and other metals culminated in the development of a new material known as metal matrix composites, or MMC [8].

The Al matrix alloy reinforced with B_4C and SiC particulate is one of the most advanced materials available [9, 10]. Because of their potential improvement in mechanical qualities such as hardness and tensile strength, which are favorable properties in tribological applications, hard materials are widely utilized as reinforcements. Reinforcements with appropriate particles increase mechanical performance in general. Graphite, alumina, and boron carbide fibers or particulates have also been considered as reinforcing materials in MMC due to their high strength and low density. [11, 12]. Aluminium MMCs, which are produced using solidification processes with boron carbide and graphite particulate as reinforcing materials, represent a class of low-cost, custom-made materials for a variety of technical applications in the automobile industry, such as brake pads, bushes, and bearings. The aluminium metal matrix material with ceramic reinforcement has the potential to develop a material with increased remarkable mechanical capabilities, thermal conductivity and high-temperature damping behavior [13, 14]. However, there is difficulty in wettability between aluminium and the ceramic reinforcement, and oxidation of the ceramics at high temperatures lead to manufacturing difficulties and cavitation's in the material.

Several researchers have investigated properties of metal matrix composites by using aluminium, copper, zinc, magnesium and lead as a base matrix. Most commonly used particulate reinforcements are SiC, TiC, Al_2O_3, B_4C, Graphite, Mica, WC and Si_3N_4 etc [15, 16].

Dinesh Patidar et al. [17] has conducted survey on boron carbide (B_4C) effect when reinforced in aluminium alloy 7075, B4C was added in weight percentage of steps 5, 10, 15 and 20 percentage and was developed by ultrasonic stir casting method, the effect of B_4C resulted in drastic increase of hardness value until 10% of B_4C and hardness for 15% and 20% showed increase in hardness with lower value. The breaking load, ultimate and flexural strength also increased with increase in B_4C particulates. Also, the rate and volume of wear of developed composite increased with decrease in weight percentage of B_4C at same load and sliding velocity.

By using the stir casting method, Veereshkumar [18] and coworkers explore the mechanical and tribological properties of Al6063 reinforced by Si_3N_4 powder. The reinforcements were varied in increments of 2 wt. percent from 0 to 10 wt. percent. The results show that raising the reinforcing percent increased monolithically and significantly the attributes like hardness and density. They claim that the composite has a greater wear resistance based on wear tests using a pin on disc configuration tribometer.

The wear rate of AA2024 with Al_2O_3/SiC/Gr produced by squeeze casting was examined by Natarayan and colleagues [19]. They optimized factors such as load (10, 20, 20N), distance (800, 1200, 1600 m), and velocity (1, 1.5, and 2 m/s) using the Taguchi method. They used an L27 orthogonal array for experimental design, and ANOVA was used to determine the impact of various components. They also used SEM with EDS to investigate wear mechanisms, surface morphologies, and composite composition. The optimal findings were anticipated using an artificial neural network

(ANN), indicating that the applied load and sliding velocity play a significant role in influencing the wear of AA2024-Al_2O_3-SiC and Gr hybrid composites. They state that in the samples, worn surface revealed adhesive wear was the most common.

However, from the literature survey, it is seen that small data is accessible as respect to the impact of variable particle size reinforcement on mechanical and wear properties of Al2618 alloy reinforced with B_4C_p composite processed by a novel two-stage liquid stirring process. With increase in demand of advanced materials in the promising modern applications, where Al-based composites are being considered as contender to supplant steel or aluminium alloys. Classic examples are cylinder liners of the vehicle motors, just as brake rotors. Al2618 alloy reinforced with B_4C_p composite is predominantly utilized in aircraft and automobile stors more specifically it is used in aerospace applications in the construction of structural frames (i.e., wing to fuselage attachment root fittings and bulk head) have increased with the advent of advanced liquid stirring process. However there is a need to develop new formulation and evaluation of its properties. Hence, an attempt has been made in the current work to develop Al2618 alloy with 2, 4, 6 and 8 wt. % of B_4C reinforced composites. Thus developed composites were exposed to microstructural characterization, mechanical and wear behavior analysis as per ASTM methods.

EXPERIMENTAL DETAILS

Preparation of the composites

By using the stir casting method, metal composites with 2, 4, 6, and 8 wt. percent B_4C (63 μm) were developed. As illustrated in Fig. 1, an Al2618 alloy was employed as the primary material, with B_4C particles (63 μm) serving as reinforcements. Tab. 1 shows the chemical composition of the alloy employed in this experiment.

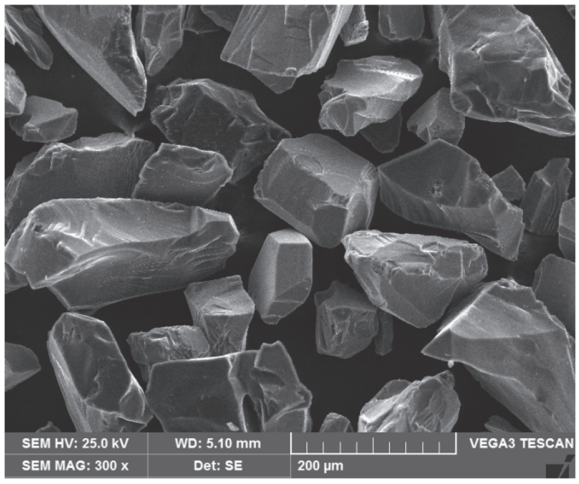

Figure 1: SEM micro-photograph of 63 micron sized B_4C particles.

Zn	Mg	Si	Fe	Cu	Ni	Mn	Cr	Al
0.1	1.8	0.2	1.3	2.7	0.9	0.3	0.1	Balance

Table 1: Chemical Composition of Al2618 alloy by weight %.

The liquid stir casting technique was used to manufacture Al2618 alloy with 63 micron size reinforced B_4C composites. The electric furnace is loaded with a predetermined weight of Al2618 alloy blocks. Normally, aluminium alloys begin to melt about 660°C, however the metal is heated to 750°C superheated temperature. Suitable thermocouples based on the temperature range are employed to measure the melting and superheated temperatures, and these temperatures are recorded. Solid hexachloroethane (C2Cl6) [20] is used to degas the superheated molten material in the crucible for roughly three minutes. For stirring the molten metal, a fan blade kind steel rotor attached on a shaft stirrer covered with zirconia ceramic is employed. The stirrer is dipped in the melted metal to a depth of about 65 percent in the crucible, and the

metal is agitated to a degree of vortex generation by rotating the stirrer at a speed of about 300 rpm. Side by side B_4C particles equivalent to 2 wt. percent by weight of charged Al2618 are preheated in a separate heater to 400°C and injected gently into the molten metal vortex in phases while churning the molten metal. The stirring process is continued until perfect wettability between the Al2618 alloy matrix and the B_4C reinforce particles is achieved, resulting in interfacial shear strength. The molten metal comprising Al2618 alloy matrix and B_4C reinforce particles is then poured into cast iron molds of 120 mm of length and dia., of 15 mm. The same procedure is used to make composites with B_4C particles in various weight %. The prepared composites of Al2618 alloy with B_4C are shown in Fig. 2.

Figure 2: Al2618 alloy with B_4C composite.

The specimen is arranged for microstructural analysis using a SEM after casting to determine the uniform circulation of reinforcing particles in the Al2618 alloy. Microstructures of Al2618 alloy and Al2618 with different percentages of B_4C reinforced composites are captured. Microstructure specimen dimensions are 15 mm in dia., and 5 mm in height. 240, 600, and 800 grit paper are used to grind the specimen's surface. The surface is then polished with polishing paper (4 micron) for a smoother finish using a polishing machine. Following that, the samples are cleaned with distilled water to eliminate any dirt or other impurities that may have accumulated on the polished surface. Keller's reagent is utilized to etch the specimens to create a contrast surface.

The theoretical and experimental densities are used to calculate the density of the Al2618 alloy with B_4C composites. By using rule of mixture the theoretical values are predicted and using the standard weight method experimental densities is calculated.

The specimen is machined in accordance with ASTM standard E10 [21] for hardness testing. The Brinell hardness tester machine is used to test the hardness. The polished surface of the specimen is smooth. A 5 mm ball indentation is made on the sample, and a load of 250 kg is applied. The results of 5 indentations are noted on the surface of the specimen and tabulated.

The specimens are machined in accordance with ASTM standard E8 [22] to investigate the tensile behavior of Al2618 alloy and Al2618 alloy with varying weight percentages of B_4C composites. The Computerized UTM is used to test the tensile strength, investigate the behavior of Al2618 alloy reinforced hybrid composites subjected to unidirectional tension, and analyze the effect of uniform distribution. The specimen's overall length is 104 mm, 45 mm gauge length and a gauge dia., of 9 mm. This tensile test can be used to determine the mechanical behavior of as cast alloys and composites. Compression strength is calculated using the ASTM E9 standard [23]. Fig. 3 depicts the tensile test specimen.

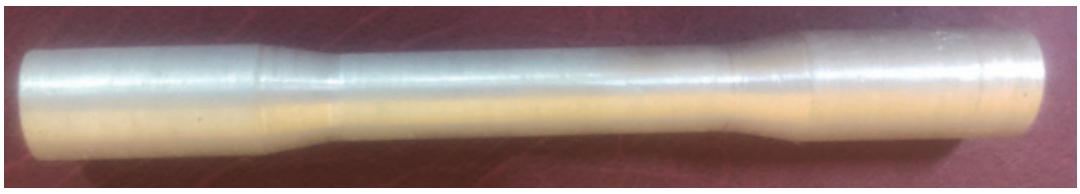

Figure 3: Tensile test specimen.

Using a pin on disc wear machine, Al2618 alloy and Al2618 with B4C reinforced composites wear behavior are investigated. The tests are carried out as per ASTM G-99 standard [24] on specimens measuring 8 mm in dia., and 30 mm in length. After performing dry sliding wear experiments at varied loads of 10 N, 20 N, 30 N, and 40 N and at 2.09 m/s sliding velocity for 3000 m sliding separation, the wear was considered. Similarly, the dry sliding wear conduct of Al2618 compound composites was investigated at 40 N load and 3000 m sliding distance at varied sliding speeds of 0.52 m/s, 1.05 m/s, 1.57 m/s, and 2.09 m/s. The height loss misfortune was reported as a wear misfortune.

Wear debris were collected during wear testing using a pin-on disc wear machine, and this debris are used to investigate distinct wear mechanisms using SEM images. Furthermore, the wear morphology of the Al2618 and Al2618 amalgam with B_4C composites was investigated using micrographs to determine the distinct wear conduct involved.

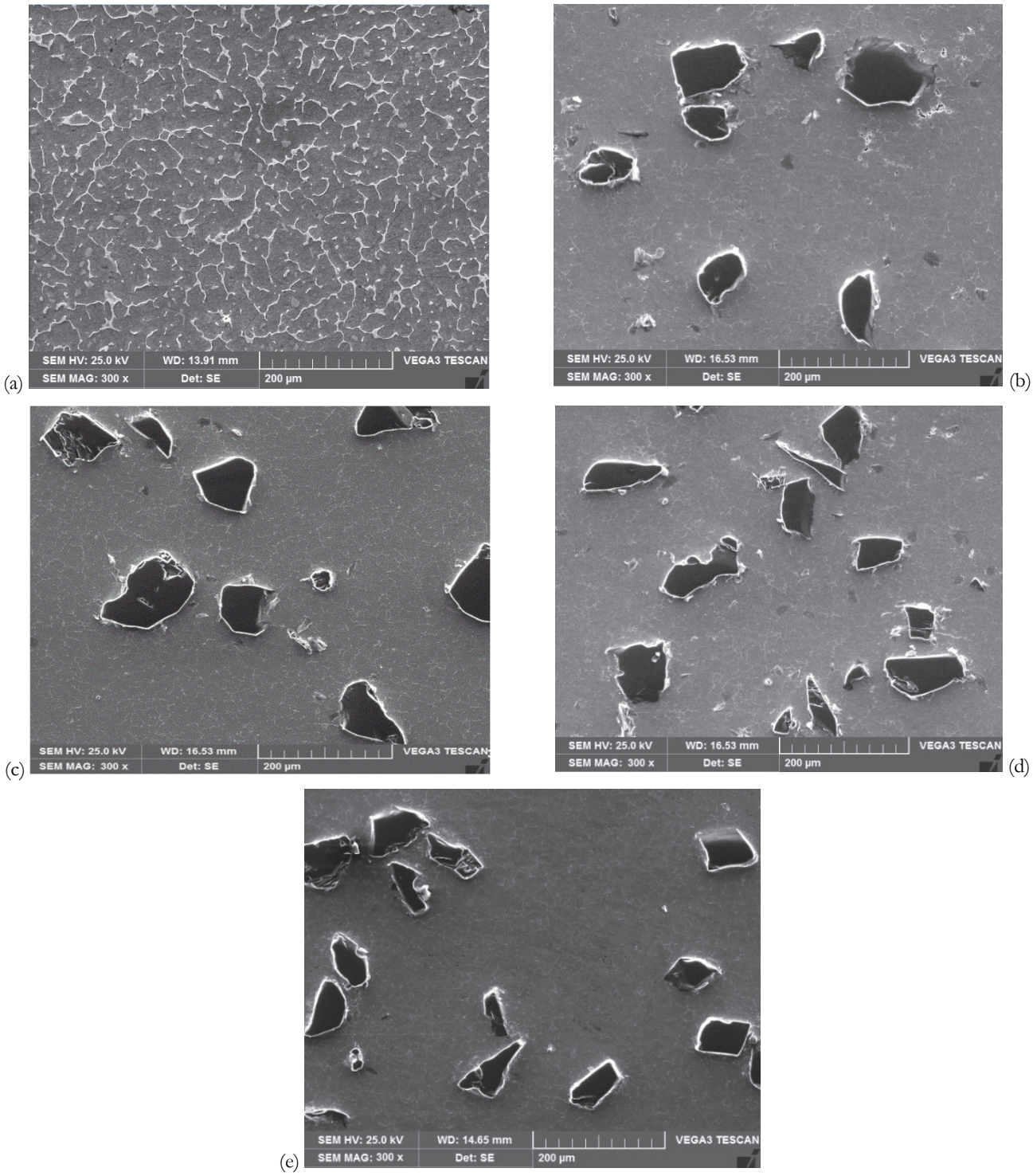

Figure 4 (a-e): SEM microphotographs of (a) as cast Al2618 alloy (bAl2618-2% B_4C (c) Al2618-4% B_4C (d) Al2618-6% B_4C (e) Al2618-8% B_4C with 63-micron B_4C particles.

RESULTS AND DISCUSSION

Microstructural studies

The microstructure of the cast Al2618 alloy is depicted in Fig. 4 (a), and it is obvious that no B_4C particles are present. SEM microstructure of Al2618-2 wt. percent 63 micron B_4C, Al2618-4 wt. percent 63 micron B_4C, Al2618-6 wt. percent 63 micron B_4C, and Al2618-8 wt. percent 63 micron B_4C reinforcement particles is depicted in Fig. 4 (b-e).

As demonstrated in Fig. 4 (b-e), the dispersion of 63 micron size B_4C reinforcement particles with varying wt. percent is almost homogenous throughout the Al2618 matrix. It also demonstrates that there are no gaps, voids, or cold closes. The B_4C reinforcement particles and the Al2618 alloy matrix have good interfacial bonding. The uniform dissemination of particles, no defects in castings, and good interfacial connection in these Al2618- B_4C particulate composites, as shown in the above SEM images, increase the complete strength of the MMC and have a significant effect on both mechanical and tribological properties.

EDS is an effective and helpful technology for determining components and their relative proportion existence. Chemical analysis can determine the existence of the elements in the sample, but it is difficult to measure the presence of proportion, hence EDS is utilized. The elemental analysis of Al2618 alloy and Al2618 and 8 wt. percent of 63 micron B4C reinforced composites is performed using the EDS technique.

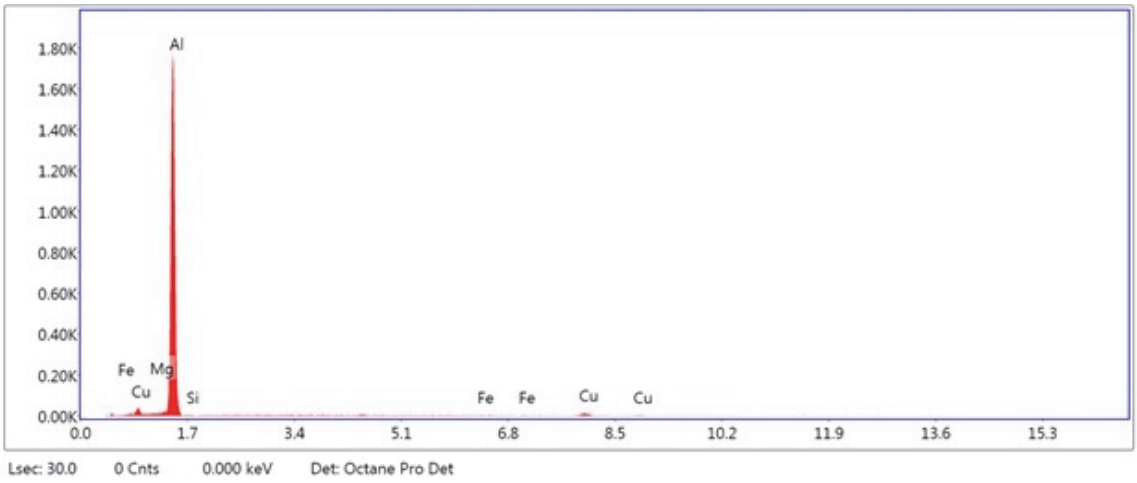

Figure 5: EDS spectrum of as cast Al2618 alloy.

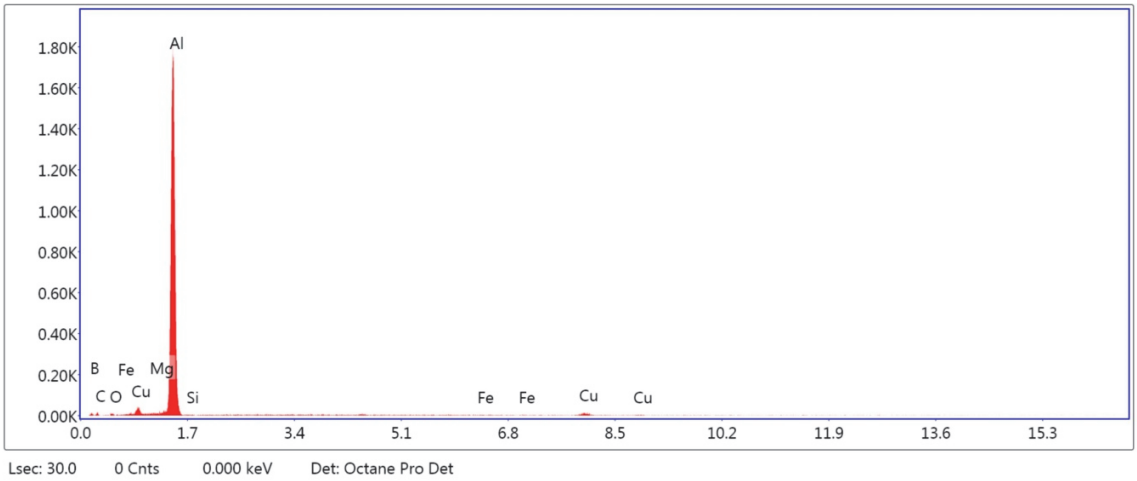

Figure 6a: EDS spectrum of Al2618-2 wt. % of B4C composites.

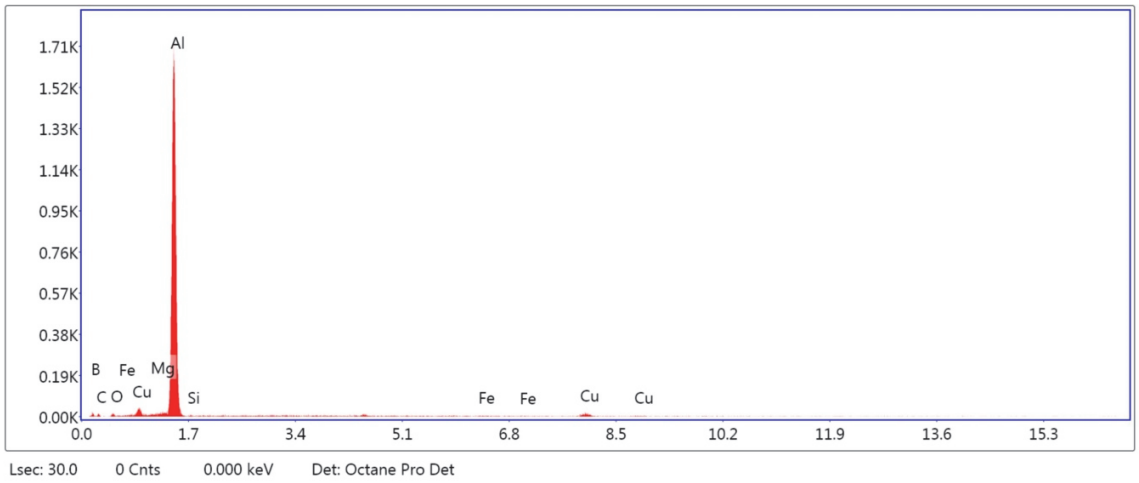

Figure 6b: EDS spectrum of Al2618-4 wt. % of B4C composites.

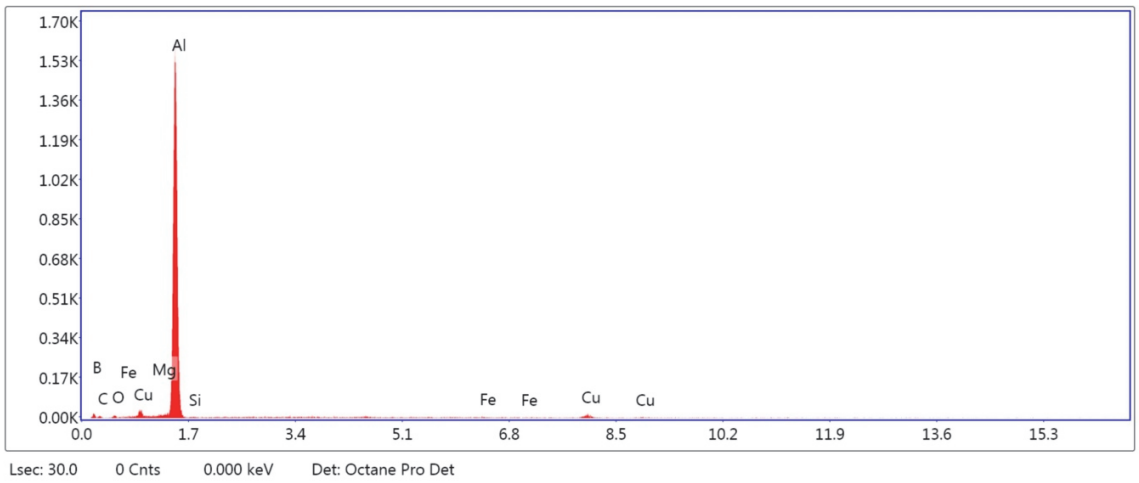

Figure 6c: EDS spectrum of Al2618-6 wt. % of B_4C composites.

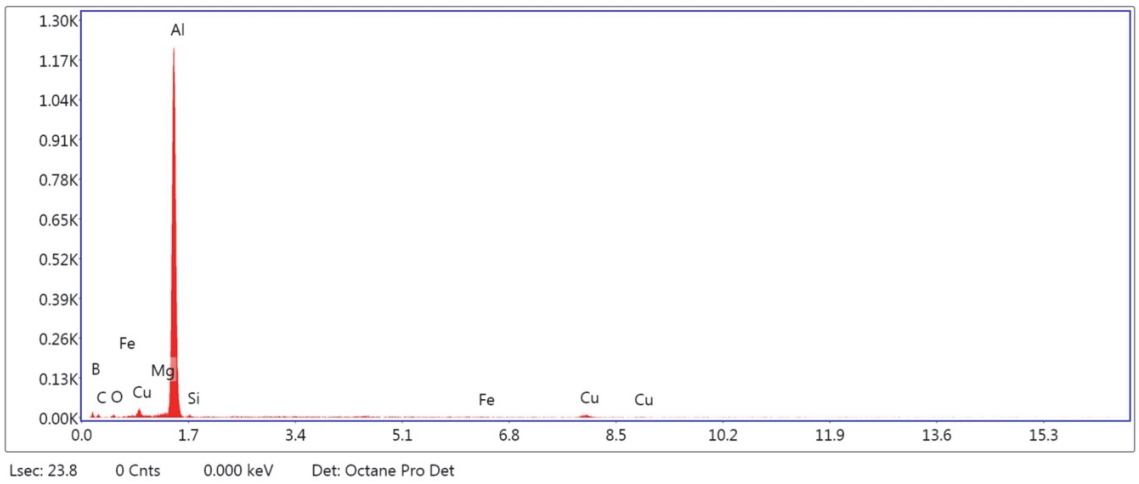

Figure 6d: EDS spectrum of Al2618-8 wt. % of B_4C composites.

Elements	Al2618	2 wt. % B_4C	4 wt. % B_4C	6 wt. % B_4C	8 wt. % B_4C
B	-	7.93	10.03	13.07	14.57
Fe	2.02	0.72	0.70	0.72	0.65
Ni	0.70	0.69	0.65	0.68	0.62
Mn	0.20	0.18	0.16	-	-
Cu	2.3	4.10	4.18	4.18	4.30
Mg	0.06	0.08	0.06	0.04	0.04
Si	0.01	-	-	-	0.06
Zn	0.19	-	-	-	-
Cr	0.83	0.79	0.77	0.69	0.80
Al	93.69	85.51	83.45	80.62	78.96

Table 2: Composition of Al2618-B_4C composites in weight % by EDS analysis.

Fig. 5 and Fig. 6(a-d) are demonstrating the energy dispersive spectrographs of Al2618 alloy and Al2618 with 2, 4, 6 and 8 weight percentages of 63 micron sized boron carbide reinforced composites. Fig. 5 is showing Al and Cu elements, this Cu element is the major alloying element in the aluminium 2XXX series alloys. Further, Fig. 6(a-d) is showing boron (B) and carbon (C) elements along with the Al peaks, which indicates occurrence of B_4C in the prepared Al2618 alloy reinforced with 2, 4, 6 and 8 wt %.B_4C composites

Fig. 7 shows the XRD pattern taken for as cast aluminium alloy Al2618 to verify its quality and standard XRD pattern. On a 2-theta scale, the peak height increases and subsequently decreases, suggesting the presence of multiple material phases. Fig. 7 shows that the peak X-ray intensities are higher at 38, 45, 65, and 78, suggesting the presence of the aluminium phase.

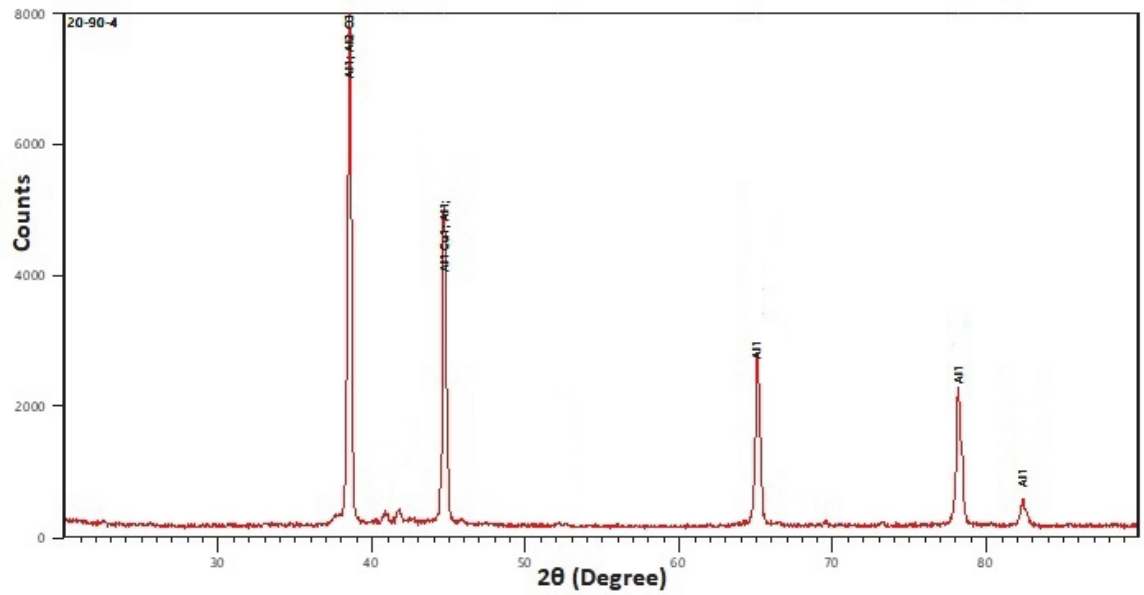

Figure 7: X-ray diffraction pattern of as cast Al2618 alloy.

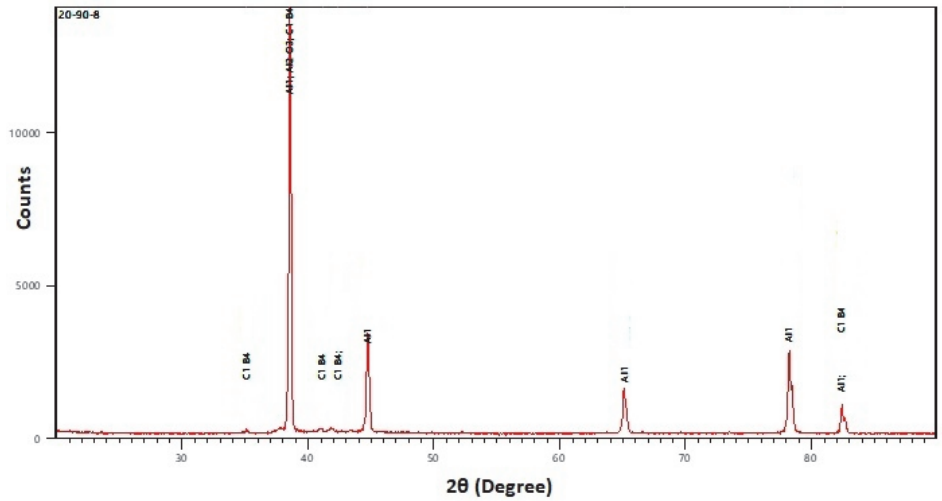

Figure 8a: X-ray diffraction pattern of Al2618 alloy with 2 wt. % of B_4C composites.

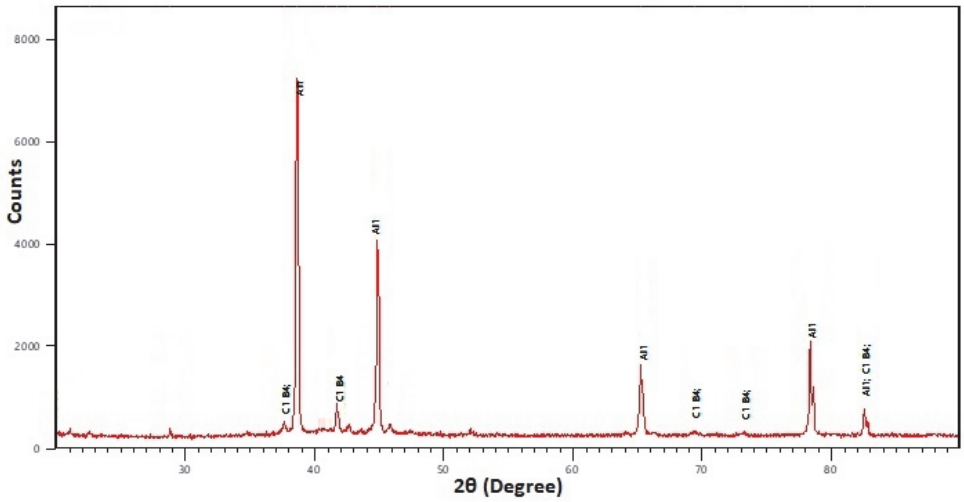

Figure 8b: X-ray diffraction pattern of Al2618 alloy with 4 wt. % of B_4C composites

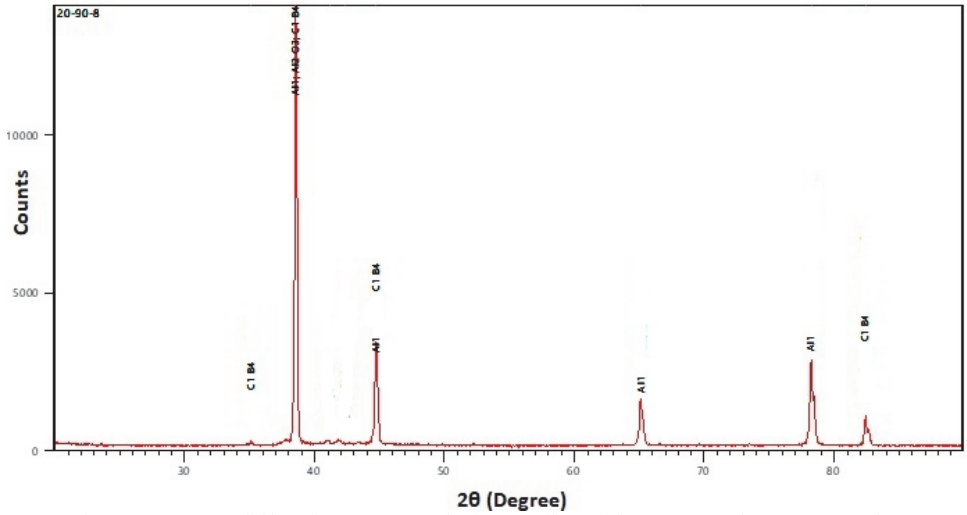

Figure 8c: X-ray diffraction pattern of Al2618 alloy with 6 wt. % of B_4C composites.

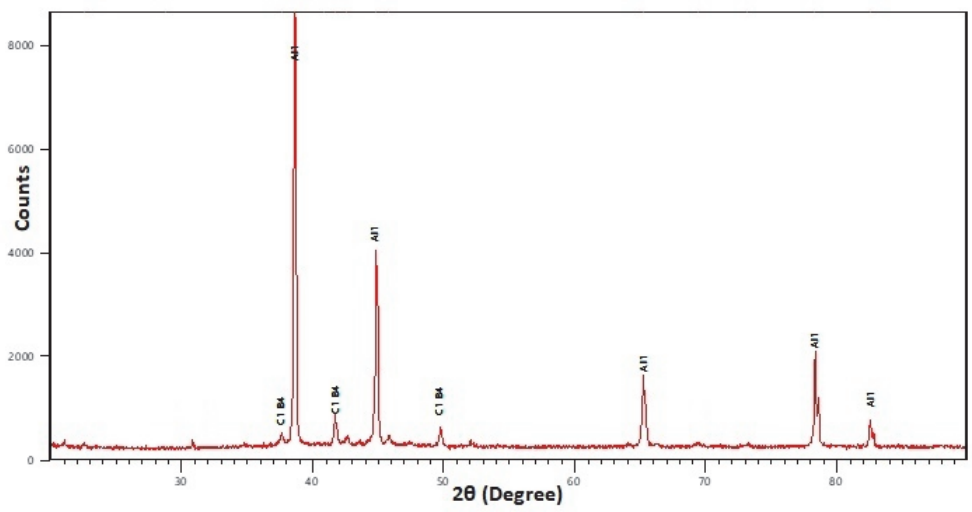

Figure 8d: X-ray diffraction pattern of Al2618 alloy with 8 wt. % of B_4C composites.

In Fig. 8(a-d) it is visible that X-ray intensities of peak are higher at 39˚, 45˚, 65˚ and 78˚ indicating the presence of aluminium phase. Along with Al phases, B_4C phases are visible at 38˚, 42˚ and 50˚.

Density Measurements

The experimental and theoretical and densities of Al2618 – 2 wt. percent B_4C, Al2618 – 4 wt. percent B_4C, Al2618 – 6 wt. percent B_4C, and Al2618 – 8 wt. percent B_4C composites are compared in Fig. 9. Aluminum alloy Al2618 has a density of 2.80 g/cm^3, while boron carbide has a density of 2.52 g/cm^3. When Al2618 is reinforced with 2 wt. percent of B_4C, the overall density of the composite decreases because B_4C has a lower density than Al2618, and Al2618 -2 wt. percent of B_4C has a density of 2.794 g/cm^3. When 4, 6, or 8% B_4C particles are used to strengthen Al2618 alloy, the theoretical density of the composite tends to be lower than that of the aluminium alloy. It's also worth noting that experimental densities are lower than theoretic densities. The decrease in density caused by the addition of B_4C is consistent with the findings of other studies [25].

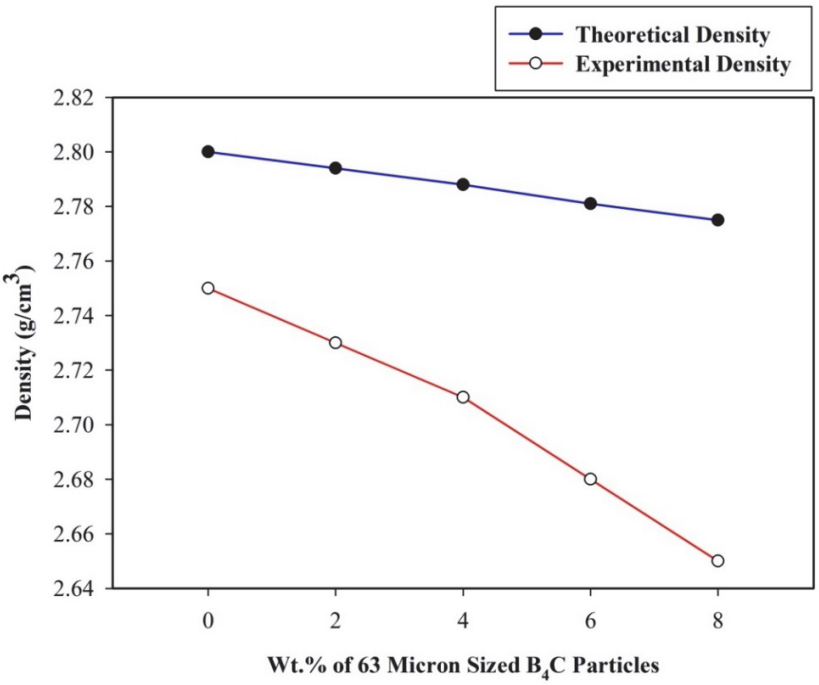

Figure 9: Theoretical and experimental densities of Al2618 with B_4C composites.

Hardness measurements

The hardness of as cast Al2618 and produced composites with different weight fractions is evaluated by Brinell hardness testing equipment utilizing 5mm ball indenter, with an applied stress of 250 kgf and dwell period of 30 seconds for each sample at different locations (see Fig. 10). The increase in hardness is attributed to the hardness of the B_4C particles, which are uniformly disseminated and contribute to the hardness of the composite by acting as barriers to the progression of dislocations within the matrix [26]. The observations and the obtained results are consistent with the results of other workers; this may be mainly due to the good connection between matrix and reinforcement.

The improvement is about 56.99% in Al2618-8 wt. % B_4C composites when compared with matrix. Same observation is found with the investigations of other researchers [27]. The increased hardness is accredited to the existence of firm B_4C particles which act as obstacle to the movement of dislocations within the Al2618 matrix. Usually, after addition of micro particles the strain energy at the peripheral of boron carbide particles is improved, so in composites enhanced hardness is found.

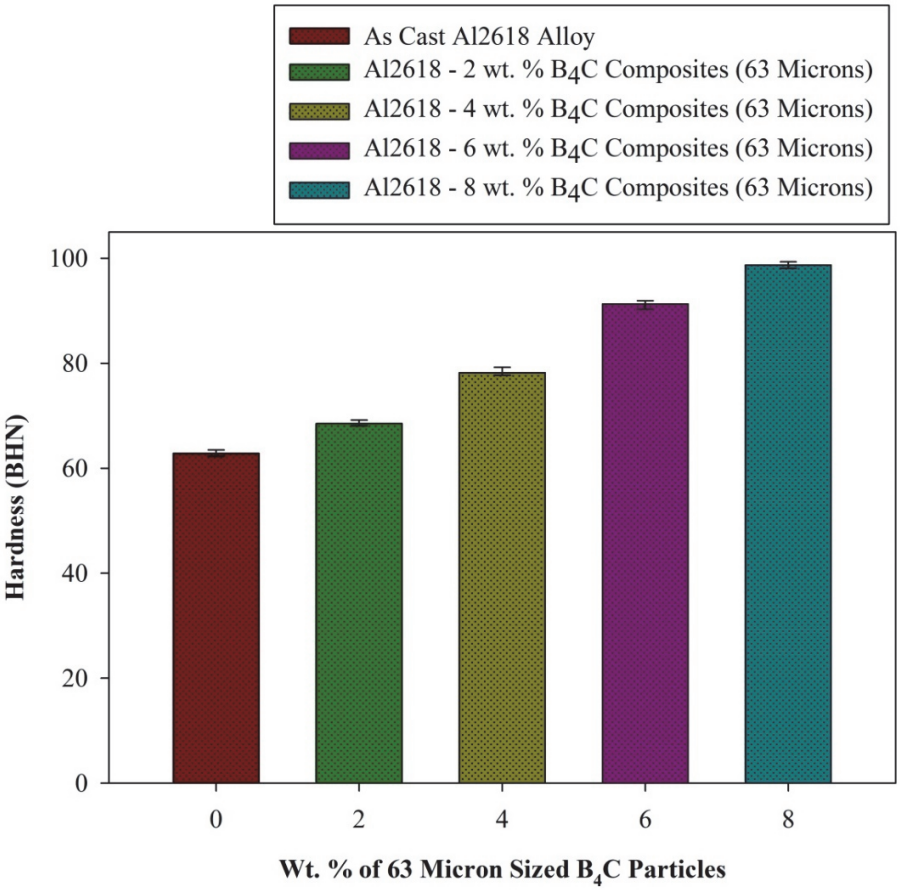

Figure 10: Hardness of Al2618 alloy with B_4C composites.

Compositions of composite samples	BHN
Al2618	62.87 ± 2.53
Al2618-2 weight percentage of B_4C	68.60 ± 3.13
Al2618-4 weight percentage of B_4C	78.47 ± 3.42
Al2618-6 weight percentage of B_4C	91.10 ± 4.32
Al2618-8 weight percentage of B_4C	98.70 ± 4.52

+ - SD (Standard Deviation)

Table 3: BHN averaged values of Al2618 and Al2618 reinforced with B_4C at different compositions (2, 4, 6 and 8 weight percentages).

Tensile properties

Figs. 11 and 12 show the results of tensile testing at room temperature with varying weight % of 63 micron sized B_4C particles. The UTS and YS increase as the percent weight fraction of reinforcing particles increases, as shown in Figs. 11 and 12.

The UTS and YS are amplified with increasing B_4C content. The B_4C particles in the alloy afford protection to the softer matrix. The UTS and YS of as cast Al2618 alloy is 185.1 MPa and 147.2 MPa respectively. Further, as weight percentage of 63 micron size B_4C particulates increased from the 2 to 8 wt. % insteps of 2 wt. %, there is increase in the UTS and YS values. It is observed that in Al2618 alloy-2 wt. % B_4C composites UTS and YS are 196.1 MPa and 158.4 MPa respectively. In the case of 8 wt. % of 63 micron size B_4C reinforced composites it is 270.8 MPa and 217.8 MPa respectively in UTS and yield strength.

Compositions of composite samples	UTS (MPa)
Al2618	185.13 ± 4.33
Al2618-2 weight percentage of B_4C	196.10 ± 4.06
Al2618-4 weight percentage of B_4C	223.37 ± 3.26
Al2618-6 weight percentage of B_4C	243.30 ± 2.67
Al2618-8 weight percentage of B_4C	270.80 ± 4.43

+ - SD (Standard Deviation)

Table 4: UTS averaged values of Al2618 and Al2618 reinforced with B4C at different compositions (2, 4, 6 and 8 weight percentages).

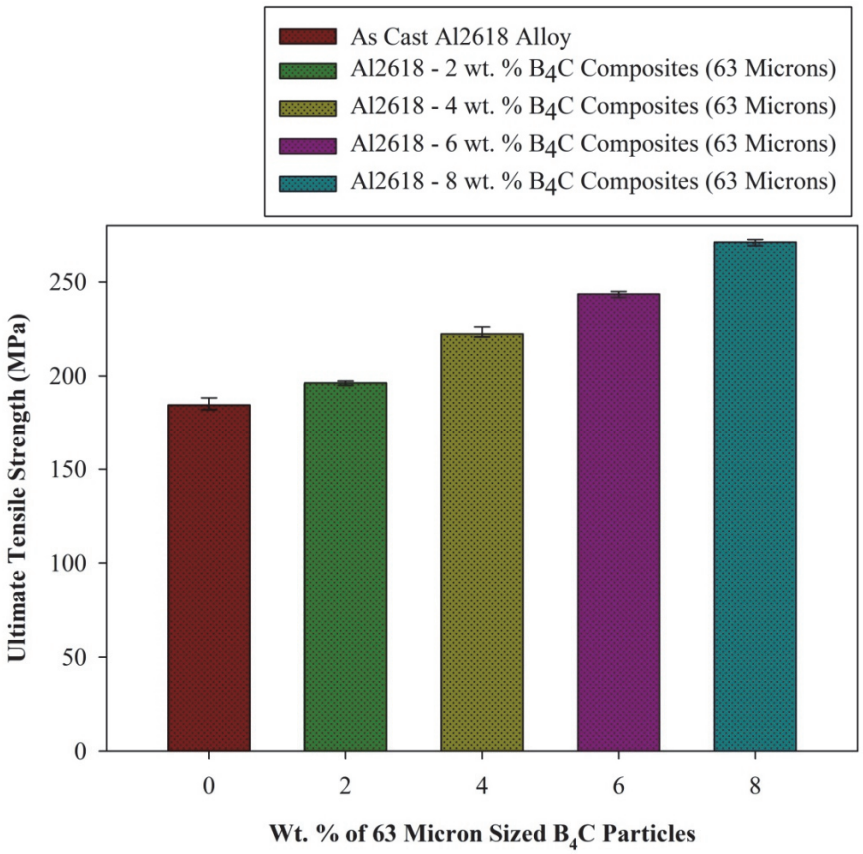

Figure 11: UTS of Al2618 alloy with B_4C composites.

Compositions of composite samples	YS (MPa)
Al2618	147.17 ± 3.18
Al2618-2 weight percentage of B_4C	158.43 ± 3.30
Al2618-4 weight percentage of B_4C	184.60 ± 3.66
Al2618-6 weight percentage of B_4C	202.93 ± 3.47
Al2618-8 weight percentage of B_4C	217.80 ± 4.09

+ - SD (Standard Deviation)

Table 5: YS averaged values of Al2618 and Al2618 reinforced with B4C at different compositions (2, 4, 6 and 8 weight percentages).

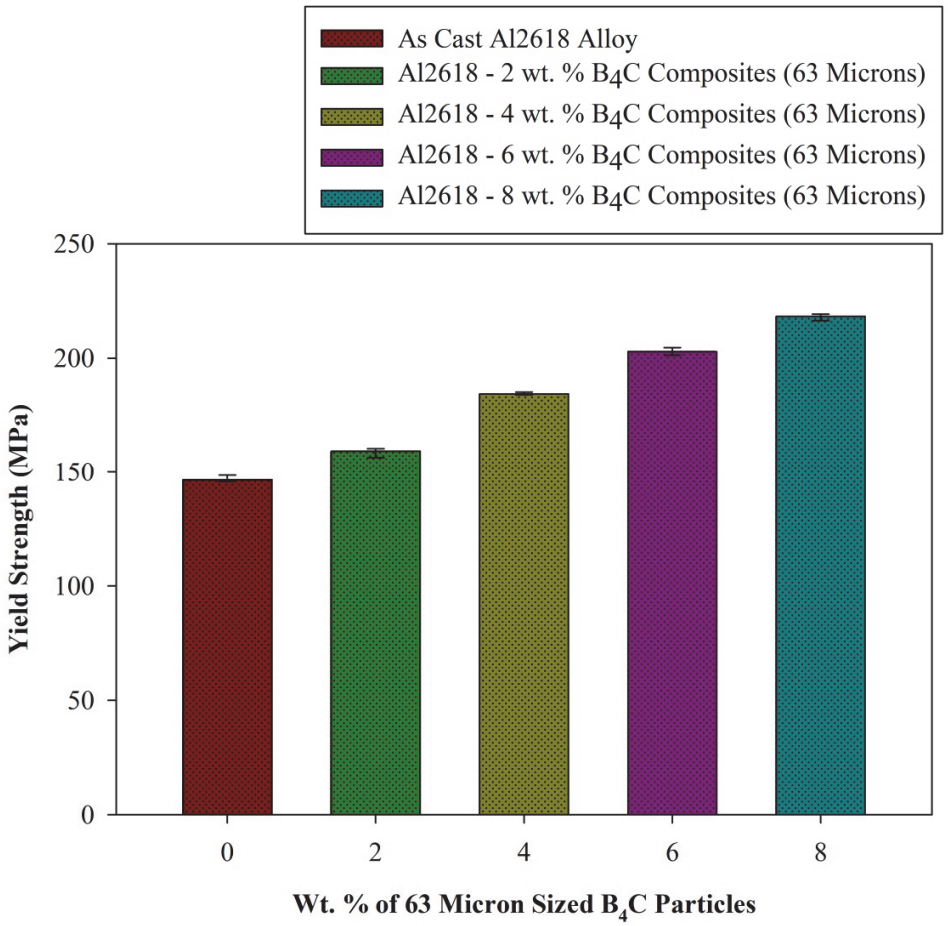

Figure 12: YS of Al2618 with B_4C composites.

The computed estimates of ultimate tensile strength were shown as a component of the weight rate of micro B_4C particles. There has been a rise in UTS when compared to base Al2618 alloy with varying wt. percent of B_4C composites. There is a significant increase in strength due to appropriate contact between the framework mixture and the supporting components. The harder the grains, the higher the hardness and also the better the quality of composites, resulting in increased wear resistance [28]. The hard ceramic B_4C particles are responsible for the increase in UTS, since they add value to the framework mixture by improving solid rigidity. Because of the difference in coefficient of developed between the flexible matrix and the brittle particles, the expansion of these hard-micro particles may have caused significant long-term compressive discomfort.

Compositions of composite samples	Percentage Elongation (%)
Al2618	13.30± 0.33
Al2618-2 weight percentage of B_4C	12.40± 0.14
Al2618-4 weight percentage of B_4C	11.27± 0.10
Al2618-6 weight percentage of B_4C	10.43± 0.17
Al2618-8 weight percentage of B_4C	9.37± 0.25

+ - SD (Standard Deviation)

Table 6: Percentage elongation averaged values of Al2618 and Al2618 reinforced with B4C at different compositions (2, 4, 6 and 8 weight percentages).

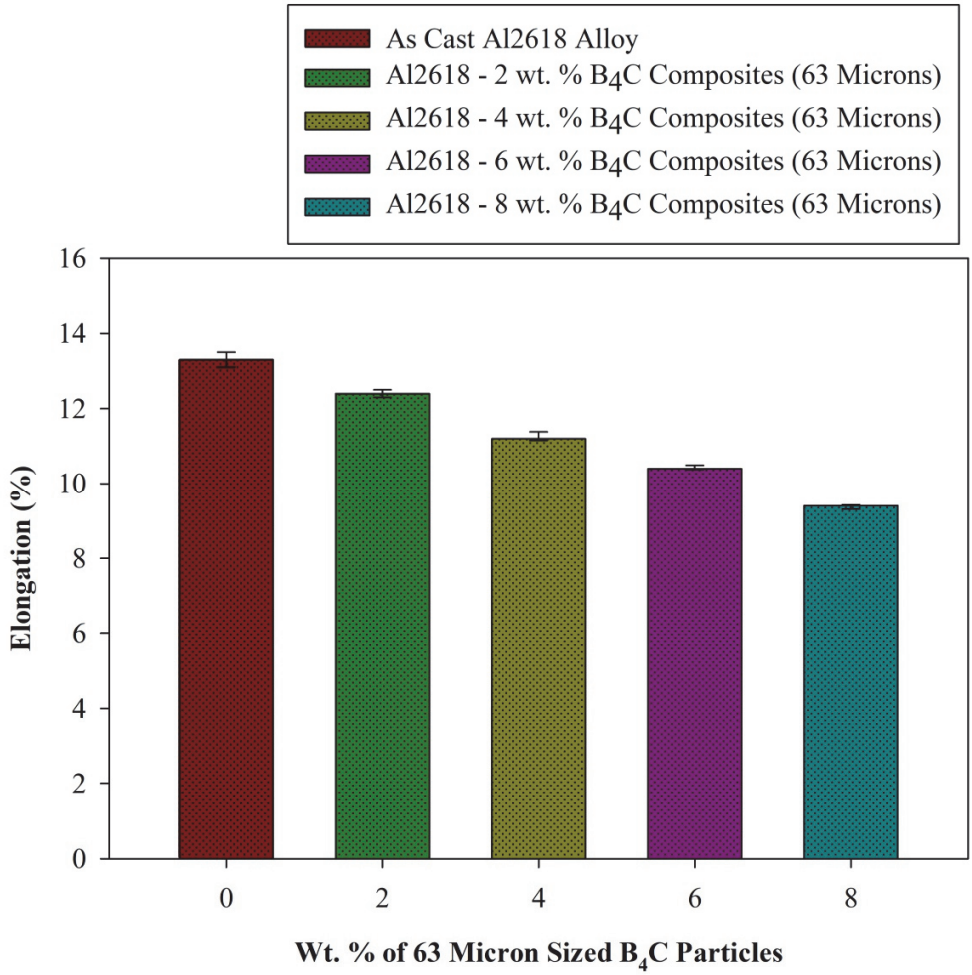

Figure 13: Elongation of Al2618 alloy with B_4C composites.

Fig. 13 indicates the effect of 63 micron size B_4C particles addition on the ductility of Al2618 alloy and its composites. The material tends to elongate when the specimen is subjected to axial load. In tensile testing, the elongation of a specimen is calculated by dividing the increase in gauge length after fracture by the original gauge length. In general, elongation of a specimen parameter is given as a percentage; the greater the percentage elongation, the greater the material's ductility. The percent elongation of as cast Al2618 alloy, Al2618 alloy with 2, 4, 6, and 8 wt. percent of 63 micron size B_4C particulates composites tested in tensile testing is shown in Fig 13. The percentage elongation of as cast Al2618 alloy is decreased after the addition B_4C particulates; it is further decreased as wt. % of reinforcement increases in Al2618 alloy. The elongation of Al2618 alloy is 13.3 %, after adding 8 wt. % of B_4C particles it is decreased to the 9.4 %. The presence of hard brittle particles in the Al2618 alloy matrix is mostly responsible for the decrease in elongation.

Compression strength

Fig. 14 is presenting the compression strength of Al2618 alloy and the composites produced with different weight percentages. From the Fig. 14 it is evident that as wt. % of B_4C increases, there is an increase in the compression strength of Al2618 alloy. The compression strength of Al2618 alloy is 538.8 MPa, in the case of Al2618 alloy-2 wt. % of B_4C, 4 wt. % of B_4C, 6 wt. % of B_4C and 8 wt. % of B_4C it is 587.5 MPa, 647.8 MPa, 717.4 MPa and 795.2 MPa respectively. Typically, the strength of ceramic particles is described in terms of compression strength rather than tensile strength. The compression strength of B_4C particles is very high as compared to the Al matrix. This behavior of reinforcement makes the material to withstand against the applied compression load. As the percentage of these particles increases in the base material, the compression load carrying capacity increased further due to area occupied by the particles is more, which resist the deformation of the matrix against the load [29].

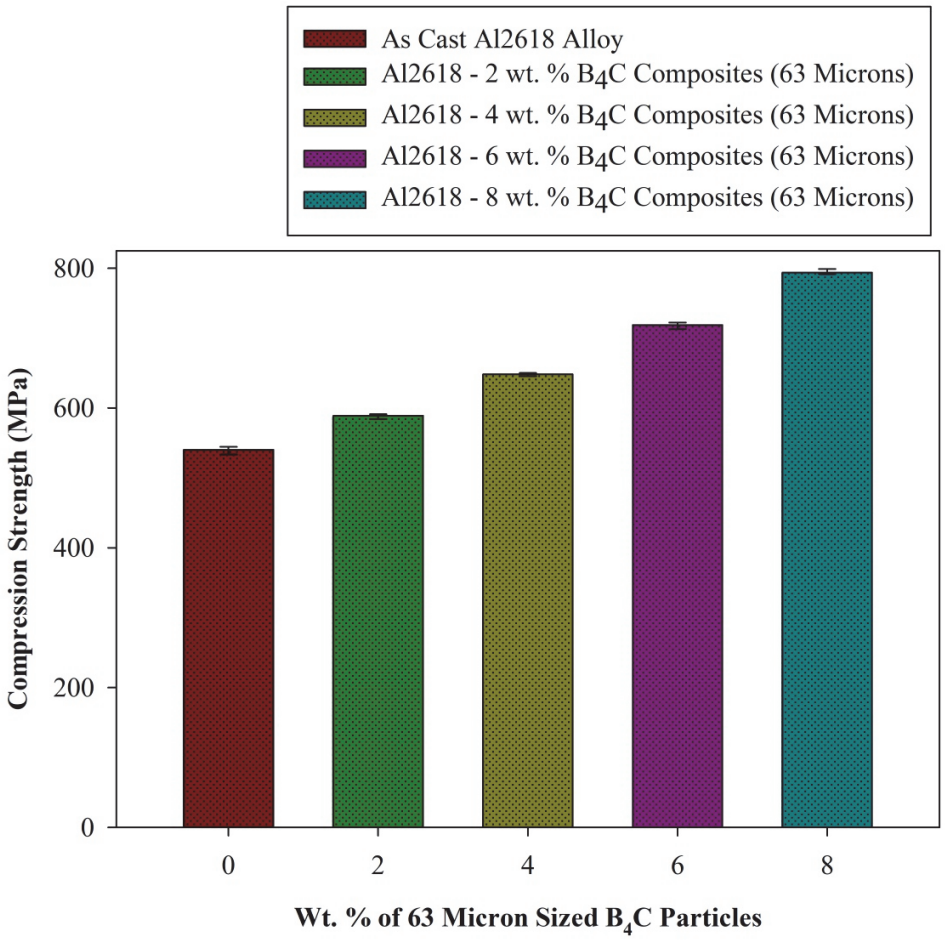

Figure 14: Compression strength of Al2618 with B_4C composites.

Compositions of composite samples	Compression Strength (MPa)
Al2618	538.83 ± 3.22
Al2618-2 weight percentage of B_4C	587.53 ± 2.81
Al2618-4 weight percentage of B_4C	647.77 ± 2.60
Al2618-6 weight percentage of B_4C	717.40 ± 3.22
Al2618-8 weight percentage of B_4C	795.17 ± 2.81

+ - SD (Standard Deviation)

Table 7: Compression strength averaged values of Al2618 and Al2618 reinforced with B4C at differentcompositions (2, 4, 6 and 8 weight percentages).

Tensile fractography

The fractured surfaces of as cast Al2618 shown in Fig 15 (a) and the fractured surfaces of Al2618 -2 wt. % of B_4C, 4 wt. % of B_4C, 6 wt. % of B_4C and 8 wt. % of B_4C composites are shown in the Fig. 15 (b-e) respectively.

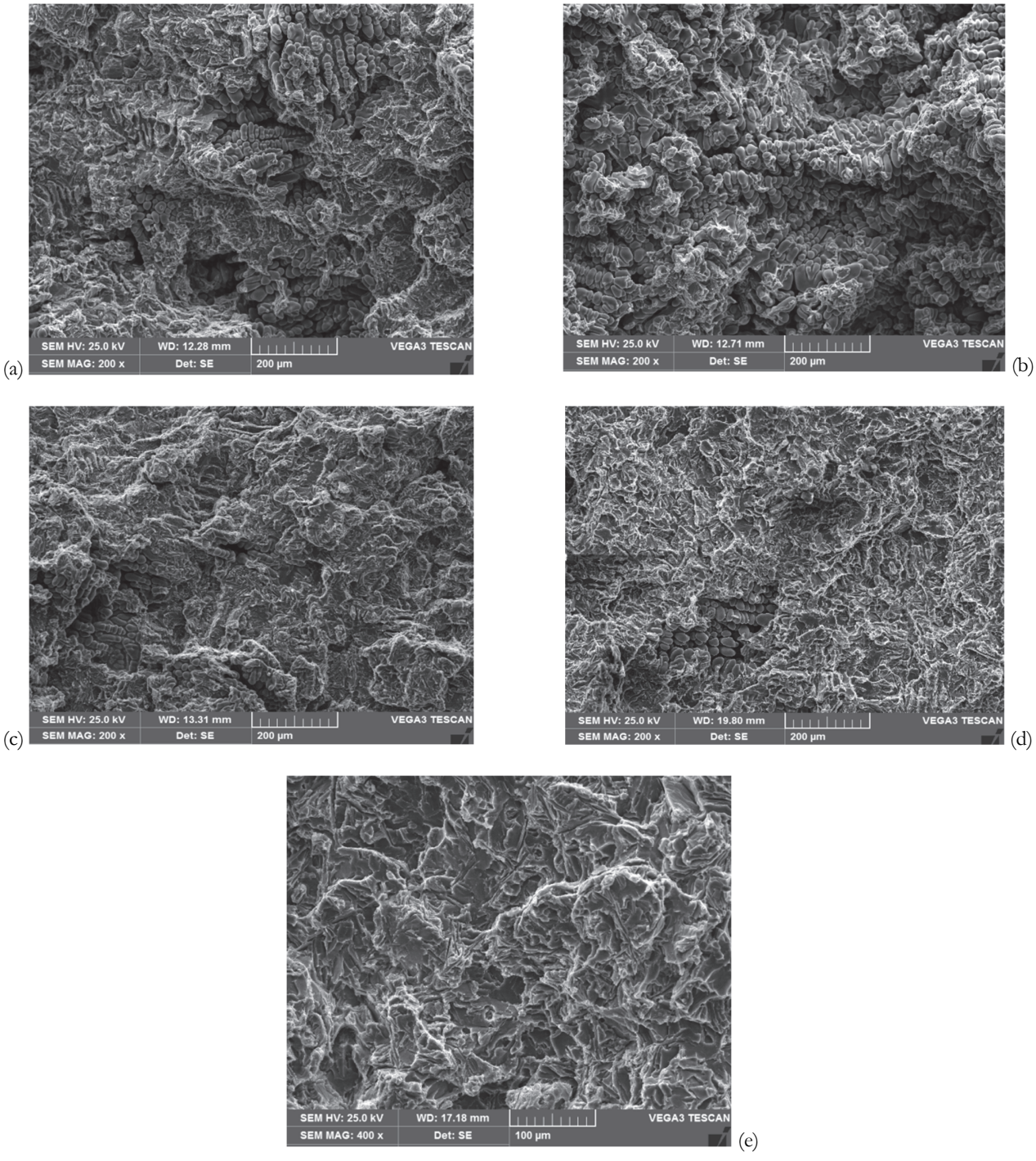

Figure 15: (a-e) SEM micrographs of tensile fractured surfaces (a) Al2618 Alloy (b) Al2618-2 wt. % B_4C (c) Al2618-4 wt. % B_4C (d) Al2618-6 wt. % B_4C (e) Al2618-8wt. % B_4C composites with 63 micron particles

The as-cast Al2618 alloy has a dimpled fracture surface, suggesting ductile fracture, but the reinforced Al2618 alloy with 2, 4, 6, and 8 wt. % has a smooth fracture surface, indicating brittle fracture. A regular dispersion of large dimples connected by bits of smaller dimples is visible in 63 micron B_4C material, exhibiting a pattern caused by ductile void growth

coalescence, although a larger proportion of B_4C composites show a pattern caused by ductile void growth coalescence. As a result, the mechanical properties of B_4C particles are anticipated to have a considerable impact on composite mechanical properties.

Wear behavior

To determine the wear properties, the test specimens of as cast Al2618 alloy, Al2618-2 wt. of 63 μm B_4C, Al2618-4 wt.% of 63 μm B_4C, Al2618-6 wt.% of 63 μm B_4C and Al2618-8 wt.% of 63 μm B_4C particles reinforced composites are prepared. The test specimens are machined according to the ASTM G99 standard for wear test.

Parameter	Load (N)	Speed (m/s)	Sliding distance (mm)	Wear in Microns (μm)				
				Al2618	2 wt%B_4C	4wt% B_4C	6 wt% B_4C	8 wt% B_4C
Varying Load	10	2.09	3000	685± 0.10	576± 0.06	509± 0.08	463± 0.05	413± 0.07
	20	2.09	3000	758± 0.07	653± 0.05	561± 0.07	502± 0.05	449± 0.05
	30	2.09	3000	809± 0.08	714± 0.06	602± 0.08	556± 0.08	487± 0.07
	40	2.09	3000	873± 0.08	778± 0.07	645± 0.06	589± 0.07	536± 0.08
Varying Sliding Speed	40	0.52	3000	679±0.08	586± 0.08	503± 0.06	457± 0.06	402± 0.04
	40	1.05	3000	726±0.06	643± 0.05	549± 0.08	485± 0.04	434± 0.05
	40	1.57	3000	782±0.05	709± 0.07	578± 0.06	543± 0.08	476± 0.07
	40	2.09	3000	864±0.07	768± 0.05	627± 0.06	557± 0.07	519± 0.06

Table 8: Wear results of Al2618 alloy and B_4C (63 microns) composites.

One of the main elements that affect wear loss is load. To better understand the wear rate of Al alloys, a lot of research has been done on the effect of normal load in wear trials. Furthermore, graphs for wear loss against varied loads of N, 20 N, 30 N, and 40 N, as well as a constant distance of 3000 m and a speed of 2.09 m/s, have been plotted to explore the influence of load on wear. The influence of load on the wear behavior of Al2618 alloy and B_4C reinforced composites is shown in Fig. 16.

The wear of all composites and the base Al2618 increases as the load increases from 10 N to 40 N, as shown in graph 16. The temperature of the sliding surface and pin surpasses the critical value with a maximum load of 40 N. As a result, the wear loss of the matrix Al2618 alloy and Al2618 alloy with 2, 4, 6, and 8 wt. percent of 63 micron B_4C composites increases as the stress on the pin increases. In all loading circumstances, the wear loss of as cast Al2618 alloy is the maximum, as shown in Fig. 16. As shown in Fig. 17, the wear loss of the composites diminishes as the wt. percent of reinforcements in the Al2618 alloy increases. The high hardness of B_4C particles, which acts as a barrier for wear loss, may explain the increase in wear resistance of the Al2618 alloy-2, 4, 6, and 8 wt. percent of 63 micron B_4C composites with increasing wt. percent of B_4C reinforcements. It can also be shown that increasing the amount of hard particles enhances wear resistance [30]; in the current research work, increasing the amount of hard B_4C particles also increased wear resistance, which is similar to the results found in the current study.

Fig. 18 depicts the wear loss as a function of speed for a variety of test materials with different compositions. The test is carried out at 0.52 m/s, 1.05 m/s, 1.57 m/s, and 2.09 m/s while maintaining a load of 40 N. It may be deduced from the above graph that f wear loss increases as the sliding speed increases. When compared to B_4C -based composite, the effect of sliding speed is greater for base Al2618 alloy.

The wear loss of Al2618 matrix alloy and B_4C composites is shown in Fig. 18 as a function of sliding speed. The loss due to wear increases as the sliding speed is raised from 0.52 m/s to 2.09 m/s for both Al2618 matrix alloy and its constituent composites.

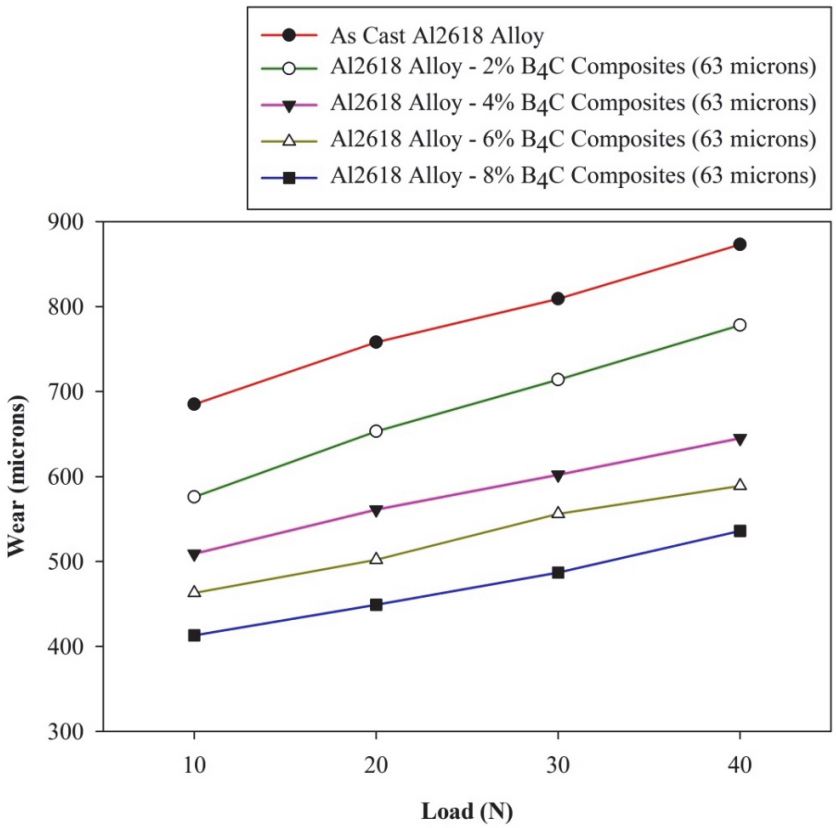

Figure 16: Shows wear loss of Al2618 Alloy and its 63 micron size B_4C reinforced composites at varying loads and 2.09 m/s constant speed

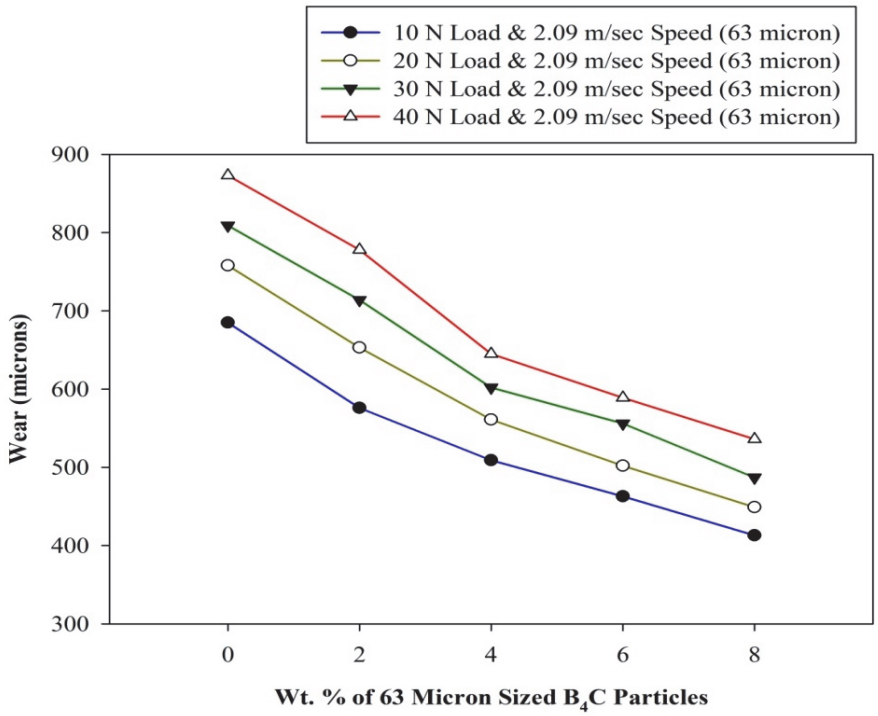

Figure 17: Wear loss of Al2618 Alloy and its 63 micron size B_4C reinforced composites at varying loads and 2.09 m/s constant speed with varying wt. % of B_4C

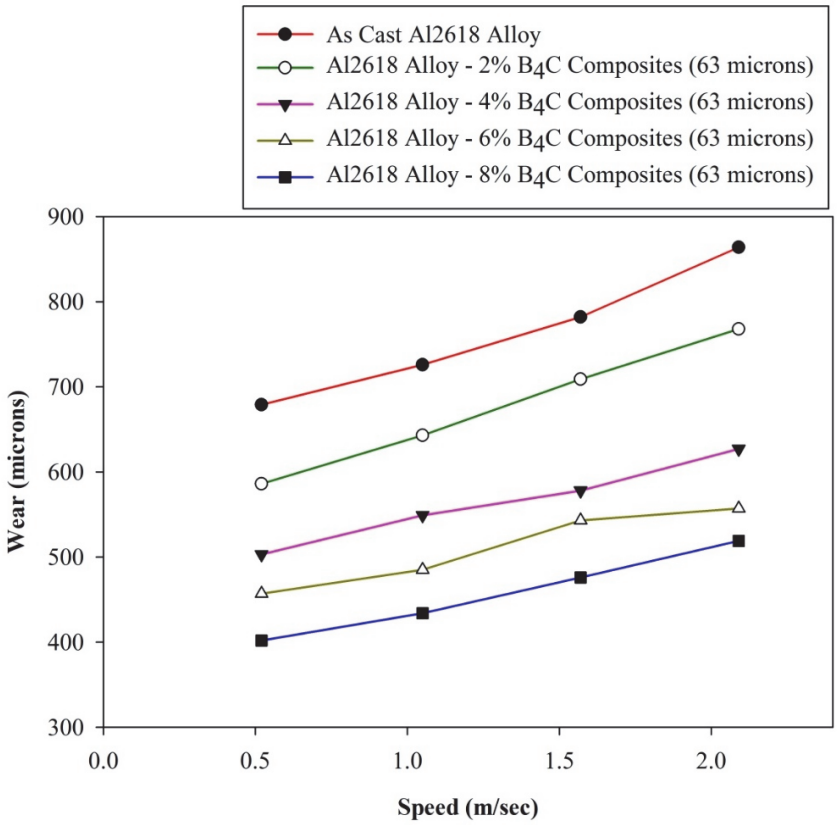

Figure 18: Wear loss of Al2618 and its 63 micron size B_4C composites at varying speeds and 40 N constant loads.

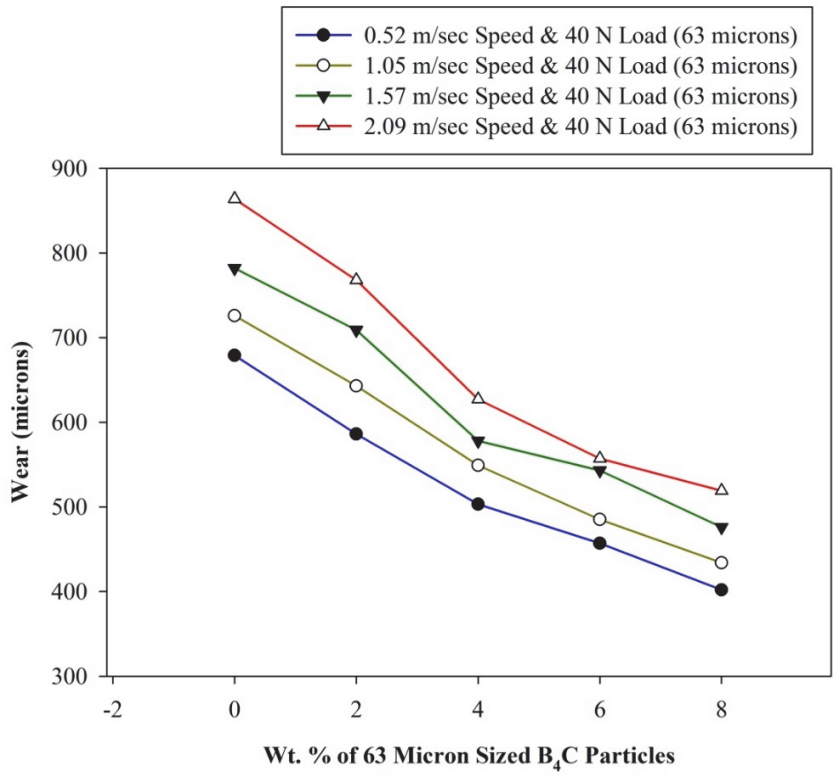

Figure 19: Wear loss of Al2618 Alloy and its 63 micron size B_4C composites at varying speeds and 40 N constant load with varying wt. % of B_4C.

Although the wear loss of the composites is substantially lower than that of the Al2618 matrix alloy at all sliding speeds, it is much lower in the case of Al2618 alloy-2, 4, 6, and 8 wt. percent 63 micron B_4C composites. In general, when the amount of B_4C particles in the composite increases, the wear loss of the composite reduces. Additionally, as the sliding speed is raised, wear loss upturns due to the composite weakening at higher temperatures due to the rubbing action [31]. Higher sliding speeds cause a rise in temperature, which causes plastic deformation of the test item [32]. As a result, there is more delamination, which leads to more wear loss. The current study's findings are similar to and consistent with earlier research conducted by other researchers. The influence of reinforcement particle size on the wear behavior of Al2618 alloy and its boron carbide reinforced composites is also shown in Fig. 19.

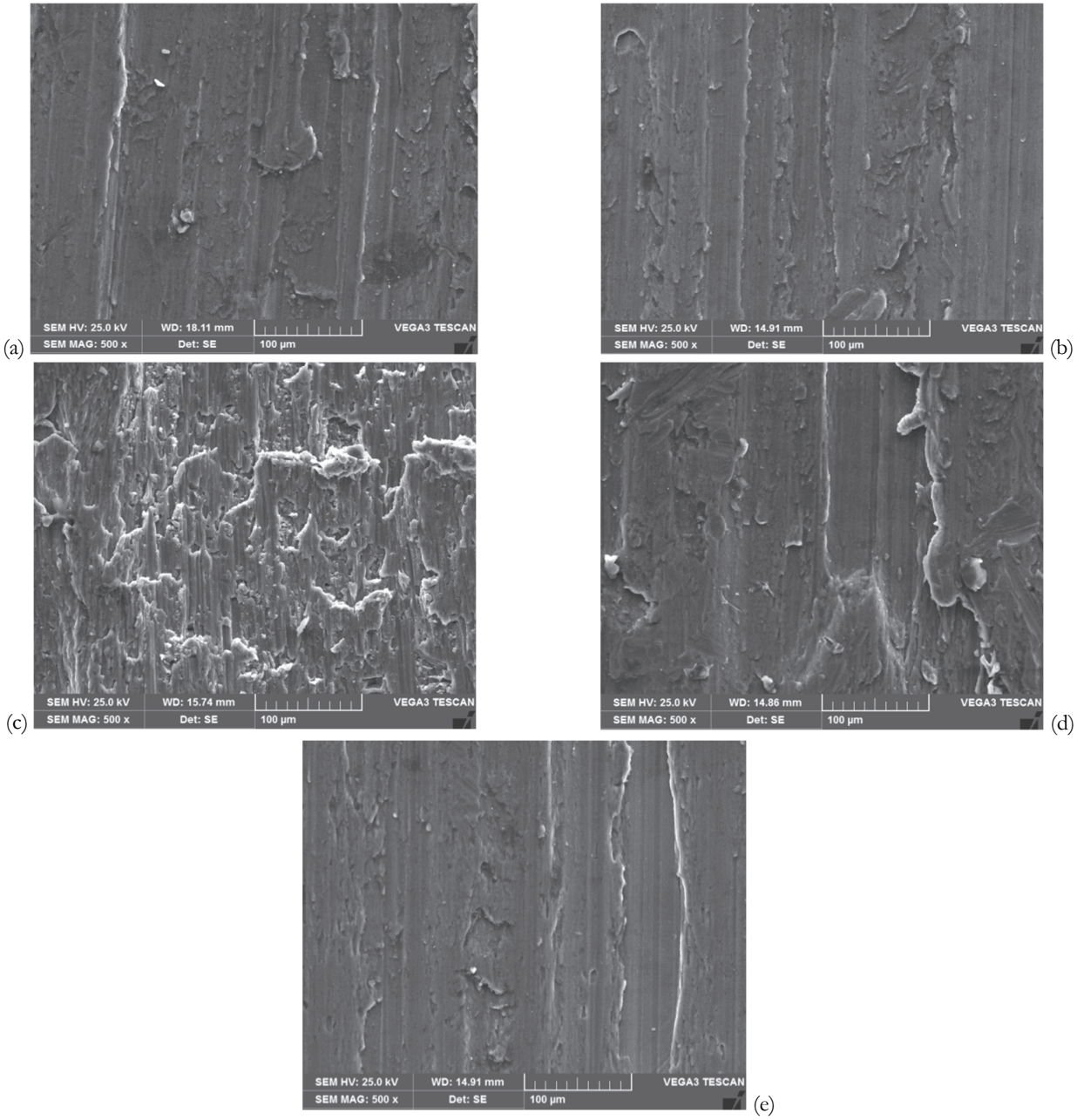

Figure 20: (a-e) Worn surfaces SEM micrographs of (a) Al2618 Alloy (b) Al2618-2 wt. % B_4C (c) Al2618-4 wt. % B_4C (d) Al2618-6 wt. % B_4C (e) Al2618-8 wt. % B_4C composites with 63 micron particles.

Wear surface morphology and wear debris

The morphology of worn-out surface of Al2618 alloy and produced composites is important to investigate because it reflects the type of wear that various materials have experienced. Since the Al2618 matrix is softer against the rotating disc

material, viscous flow in the form of a pin occurs during sliding, causing malleable deformation of the sample surface and considerable material loss. As shown in Fig. 20 (a), the worn surface of Al2618 alloy has grooves, micro-pits, and a fractured oxide layer, which would have exacerbated wear loss. The grooves or erosion in Al2618 alloy with different wt. percent 63 micron B_4C composites have decreased with increasing B_4C particles, as shown in Fig 20 (b-e), indicating that there is greater and more resistance to wear loss [33]. Meanwhile, when B_4C particles are enlarged, it appears that stress is transferred to them, strain concentration occurs around them, and the worn surface area has fewer cracks and grooves.

(a) 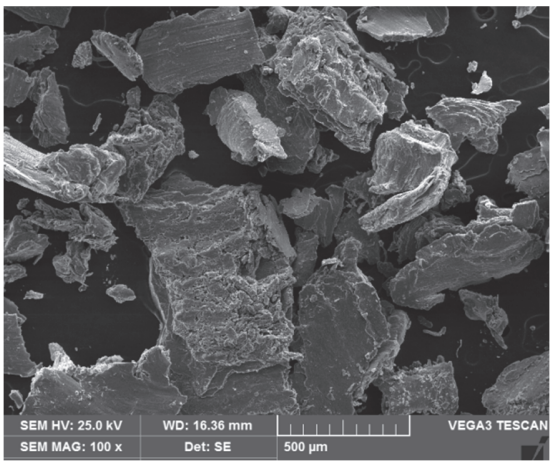

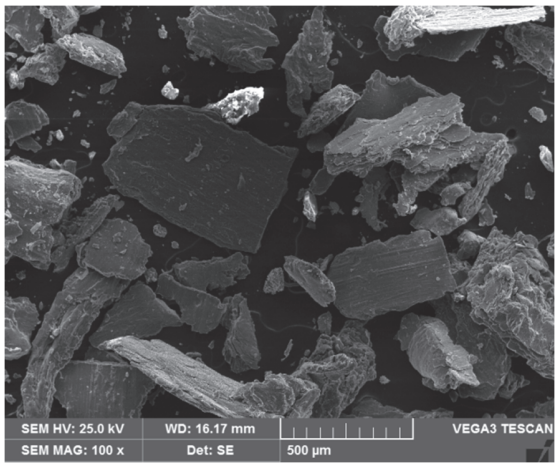

(b)

Figure 21 (a-b): Wear debris SEM micrographs of (a) Al2618 Alloy (b) Al2618-8 wt. % B_4C composites with 63 micron particles.

Fig. 21 (a) depicts debris created by Al2618 aluminium alloy wear. The size of the debris produced by the wear mechanism illustrates the level of wear suffered by the Al2618 alloy. Because the extended layers formed by the worn surface could not withstand the enormous load, they were dragged and hurled out in the form of thin plates. The ductility of the test sample was responsible for the formation of these thin extended mechanical layers. In Fig 21, wear debris of Al2618 alloy-8 wt % 63 micron B_4C composites can be visible as particles crushed between the test pieces and revolving disc (b). Small particles, such as shards pushed out of the pin, show less wear in the wear debris of B_4C -based composites (test piece). In comparison to Al-B_4C composites, the size and type of debris in Al2618 alloy explains the level of wear.

Conclusions

The stir cast route effectively produces the Al2618 alloy with 63 micron sized B_4C particles MMCs with 2, 4, 6, and 8 wt. percent. The SEM micrographs show that the B_4C particles are dispersed uniformly in the Al2618 alloy. The EDS study exposed the occurrence of B_4C particles in manufactured composites, and the XRD patterns of Al2618 alloy containing 8 weight percentages of B_4C composites were examined. The presence of B4C phases in the Al2618 alloy matrix is confirmed by XRD investigation. The theoretical and actual densities of Al2618 alloy with 2, 4, 6, and 8 wt. percent B_4C composites reduced with the insertion of B_4C particles in the matrix alloy. B_4C reinforced composites hardness; UTS, YS, and compression strength have increased with a slight increase in ductility. The various fracture mechanisms of the base alloy Al2618 alloy and produced composites were revealed by fractographic analysis of tensile ruptured surfaces using SEM. The wear resistance of Al2618 alloy has been improved by the addition of B_4C particles. The worn surface morphology and wear debris of Al2618 alloy and B_4C composites reveal a variety of wear mechanisms.

References

[1] Pankaj, J. R., Sridhar, B.R., Nagaral, M., and Jayasheel, H. I. (2020). Mechanical behavior and fractography of graphite and boron carbide particulates reinforced A356 alloy hybrid metal matrix composites, Advanced Composites and Hybrid Materials, 3, pp. 114-119.

[2] Prasad, N.H., Srinivas, H.K., Nagaral, M. (2019). Characterization of tensile fractography of nano ZrO2 reinforced copper-zinc alloy composite, Frattura ed Integrity Strutturale (Fracture and Structural Integrity), 48, pp. 370-376.

[3] Nagaral, M., Shivananda, K., Auradi, V., and, Kori, S. (2018). Mechanical characterization of ceramic nano B4C-Al2618 alloy composites synthesized by semi solid processing, Transactions of the Indian Ceramic Society, Vol.77, No.3, pp. 1-4.
[4] Siddesh Kumar, N. G., Shivashankar, G. S., Basavarajappa, S., Suresh, R. (2017). Some studies on mechanical and machining characteristics of Al2219/n-B4C/MoS2 nano hybrid metal matrix composites, Measurement, 107, pp. 1-11.
[5] Ramesh, C. S., Noor Ahmed, R., Mujeebu M. A., Abdullah M. Z. (2009). Development and performance analysis of novel cast copper SiC-Gr hybrid composite, Materials and Design, 30, pp. 1957-1965.
[6] Bharath, V., Nagaral, M., Auradi, V. (2012). Preparation, characterization and mechanical properties of Al2O3 reinforced 6061 Al particulate MMC, International Journal of Engineering Research and Technology, 1, 6, , pp. 1-6.
[7] Vijaykumar, H., Dundur, S. T., Bharath, R. L., Rajesh, G. L., and Auradi, V. (2014). Studies on mechanical and machinability properties of B4C reinforced 6061 aluminium MMC produced via melt stirring, Applied Mechanics and Materials, 592, pp. 744-748.
[8] Manjunatha, R., Kempaiah, D., Ravishankar, Panduranga, G., Setty, M., Rakesh, S., Mallappaji, C., Prasad, S., Kumar, R. (2019). Evaluation on Microstructure and Mechanical Behaviour of Al6061-Al2O3-Gr Hybrid Composites, Open Journal of Composite Materials, Vol.9 No.3, 285-299 10.4236/ojcm.2019.93017
[9] Pankaj, A.P., and Barve, S.B. (2022). Enhanced microstructure and mechanical properties of Al6061 alloy via graphene nanoplates reinforcement fabricated by stir casting, Funct. Compos. Struct. 4, https://doi.org/10.1088/2631-6331/ac586d
[10] Singh, J., and Chauhan, A. (2019). A review of microstructure, mechanical properties and wear behavior of hybrid aluminium matrix composites fabricated via stir casting route. Sådhanå ; 44:16, Indian Academy of Sciences, https://doi.org/10.1007/s12046-018-1025-5
[11] Kumar, H S., Kempaiah, U.N., Nagaral, M., and Auradi, V. (2021). Impact, Tensile and Fatigue Failure Analysis of Boron Carbide Particles Reinforced Al-Mg-Si (Al6061) Alloy Composites, Journal of Failure Analysis and Prevention, 21, 6, pp. 2177-2189.
[12] Reddy, A., Chennakesava. (2011). Tensile fracture behaviors of 7072/SiCp metal matrix composites fabricated by gravity die casting process, Materials Technology, 26, 5, 257.
[13] Wang, R M., Surappa, M K., Tao, C H., Li, C Z., Yan, M G. (1998). Microstructure and interface structure studies of SiC reinforced Al6061 metal matrix composites", Materials Science and Engineering A, 254, pp. 219-226.
[14] Sajjadi, S A., Torabi P.M., Ezatpour, H.R., Sedghi, A. (2014). Fabrication of A356 composite reinforced with micro and nano Al2O3 particles by a developed compo-casting method and study of its properties, Journal of Alloys and Compounds, 511, pp. 226-231.
[15] Chandrasekhar, G.L., Vijayakumar, Y., Nagaral, M., Anilkumar, C. (2021). Microstructural Evaluation and Mechanical Behaviour of Nano B4C Reinforced Al7475 Alloy Metal Composites, International Journal of Vehicle Structures and Systems, 13, 5, pp. 673-677.
[16] Nagaral, M., Auradi, V., Kori, S.A., Reddappa, H.N., Jayachandran, Veena, S. (2017). Studies on 3 and 9 wt. % of B4C particulates reinforced Al7025 alloy composites, AIP conference proceedings, 1859, 1, 020019.
[17] Dinesh, P., Rana, R S. (2017). Effect of B4C reinforcement on the various properties of aluminium matrix composites: a survey paper, Materials Today Proceedings, 4, pp. 2981-2988.
[18] Veereshkumar, G. B. (2019). Assessment of mechanical and tribological characteristics of Silicon Nitride reinforced aluminium metal matrix composites, Composites Part B: Engineering, 175, 107138.
[19] Natarayan, L. (2021). Chapter Ten-Optimization of wear parameters of aluminium hybrid metal matrix composites by squeeze casting using Taguchi and artificial neural network, Sustainable Manufacturing and Design, 17, pp. 223-234.
[20] Jayasheel, H.I., Sridhar, B. R., Vitala, H R., Pankaj, J.R. (2015). Wear behavior of Al2219-TiC particulate metal matrix composites, American Journal of Materials Science, 5, 3C, pp. 34-37.
[21] Vasanthkumar, H.S., Kempaiah, U.N., Nagaral, M., and Revanna, K. (2021). Investigations on mechanical behaviour of micro B4C particles reinforced Al6061 alloy metal composites, Indian Journal of Science and Technology, 14, 22, pp. 1855-1863.
[22] Nagaral, M., Auradi, V., Bharath, V. (2021). Mechanical characterization and fractography of 100 micron sized silicon carbide particles reinforced Al6061 alloy composites, Metallurgical and Materials Engineering, https://doi.org/10.30544/639.
[23] Anjan, B.V. A., Saravanan, R., Raviprakash, M., Nagaral, M. (2021). Microstructure, Tensile and Flexural Strength of Boron Carbide Particles Reinforced Al2030 Alloy Composites, Indian Journal of Science and Technology, 14, 28, pp. 2342-2350.

[24] Matti, S., Shivakumar, B P., Shashidhar, S., Nagaral, M. (2021). Dry sliding wear behavior of mica, fly ash and red mud particles reinforced Al7075 alloy hybrid metal matrix composites, Indian Journal of Science and Technology, 14, 4, pp. 310-318.
[25] Rajmohan, T., Palanikumar, K., Ranganathan, S. (2013), Evaluation of mechanical and wear properties of hybrid aluminium matrix composites, Transactions of Nonferrous Metals Society of China, 23, pp. 2509-2517.
[26] Kalaiselvan, K., Murugan, N., Parameshwaran, S. (2011). Production and characterization of AA6061-B4C stir cast composite, Materials and Design, 32, pp. 4004-4009.
[27] Varol, T., Canakci, A., and Ozsahin, S. (2013), Artificial neural network modeling to effect of reinforcement properties on the physical and mechanical properties of Al2024-B4C composites produced by powder metallurgy, Composites Part B, 54, pp. 224-233.
[28] Kumar, N., Kumar, R., Gautham, Mohan, S. (2015). In situ development of ZrB2 particles and their effect on microstructure and mechanical properties of AA5052 metal matrix composite, Materials and Design, 80, pp. 129-136.
[29] Patidar,D., and Rana, R. S. (2017). Effect of B4C reinforcement on the various properties of aluminium matrix composites: a survey paper, Materials Today Proceedings, 4, pp. 2981-2988.
[30] Pankaj, J. R., Nagaral, M., Rachoti, S., Jayasheel, H. (2020). Impact of boron carbide and graphite dual particulates addition on wear behavior of A356 alloy metal matrix composite, Journal of Metals, Materials and Minerals, 30, 4, pp. 106-112.
[31] Mindivan, H. (2010). Reciprocal sliding wear behavior of B4C particulate reinforced aluminium alloy composites, Material Letters, 64, pp. 405-407.
[32] Al-Salihi, H.A., Mahmood, A. A., and Alalkawi, H. J. (2019). Mechanical and wear behavior of AA7075 aluminum matrix composites reinforced by Al2O3 nanoparticles, Nano composites, 5:3, 67-73, DOI: 10.1080/20550324.2019.1637576
[33] Sharma, S., Kini, A., Shankar, G., Rakesh, T. C., Raja H. (2018). Tensile fractography of artificially aged Al6061-B4C composites, Journal of Mechanical Engineering and Sciences, 12, 3, pp. 3866-3875.